


## FIRe glider: Mapping in situ chlorophyll variable fluorescence with autonomous underwater gliders

Filipa Carvalho <sup>1\*</sup>, Maxim Y. Gorbunov <sup>2</sup>, Matthew J. Oliver <sup>3</sup>, Christina Haskins <sup>2,4</sup>, David Aragon,<sup>2</sup>  
Josh T. Kohut <sup>2</sup>, Oscar Schofield <sup>2</sup>

<sup>1</sup>National Oceanography Centre, Southampton, UK

<sup>2</sup>Department of Marine and Coastal Sciences, Rutgers University, New Brunswick, New Jersey

<sup>3</sup>School of Marine Science and Policy, College of Earth, Ocean and Environment, University of Delaware, Lewes, Delaware

<sup>4</sup>Department of Applied Ocean Physics & Engineering, Woods Hole Oceanographic Institution, Woods Hole, Massachusetts

### Abstract

Nutrient and light availability regulate phytoplankton physiology and photosynthesis in the ocean. These physiological processes are difficult to sample in time and space over physiologically and ecologically relevant scales using traditional shipboard techniques. Gliders are changing the nature of data collection, by allowing a sustained presence at sea over regional scales, collecting data at resolution not possible using traditional techniques. The integration of a fluorescence induction and relaxation (FIRe) sensor in a Slocum glider allows autonomous high-resolution and vertically-resolved measurements of photosynthetic physiological variables together with oceanographic data. In situ measurements of variable fluorescence under ambient light allows a better understanding of the physical controls of primary production (PP). We demonstrate this capability in a laboratory setting and with several glider deployments in the Southern Ocean. Development of these approaches will allow for the in situ evaluation of phytoplankton light stress and photoacclimation mechanisms, as well as the role of vertical mixing in phytoplankton dynamics and the underlying physiology, especially in remote locations and for prolonged duration.

Phytoplankton are the foundation of all aquatic ecosystems and their photosynthetic activity and production of organic carbon not only supports highly productive ocean/lake ecosystems but also plays a significant role in shaping the chemistry of the Earth (Falkowski and Knoll 2007). Phytoplankton populations are highly dynamic with high turnover rates driven by a suite of environmental factors such as light, macronutrients, micronutrients, grazing and temperature (Falkowski and Raven 2007). Since the pioneering work by Lorenzen (1966), chlorophyll fluorometers have been widely adopted by the oceanographic community and provide sensitive non-intrusive estimates of phytoplankton biomass. While chlorophyll fluorescence is routinely used for estimating chlorophyll concentrations, conventional fluorometers do not provide insight into the physiological state of phytoplankton or their photosynthetic rates. The pump-and-probe technique (Kolber et al. 1988), the fast repetition rate (FRR) fluorometer (Kolber et al. 1998), and the fluorescence induction and

relaxation (FIRe) sensors (Gorbunov and Falkowski 2005) have been developed to study phytoplankton physiology and evaluate the environmental controls of ocean primary production. Variable fluorescence signals provide a sensitive tool to measure the optical cross-sections for photosynthesis, the quantum yields of photochemistry, and rates of photosynthetic electron transfer in phytoplankton (Falkowski et al. 2004). Variable fluorescence measurements have allowed the oceanographic community to study the underlying mechanisms and factors regulating the physiological state and growth of phytoplankton (Suggett et al. 2010). However, the application of this technology has been largely limited to sampling from ships (Lin et al. 2016), airborne (Chekalyuk et al. 2000) or diving (Gorbunov et al. 2000; Gorbunov et al. 2001) approaches, which limits when, where and how much data is collected.

Observations of horizontal distributions of near-surface phytoplankton photosynthetic properties (such as the quantum yield for electron transport) using ship-based underway fluorometers (Lin et al. 2016) and LIDARs (Light Detection and Ranging) (Chekalyuk and Gorbunov 1993) have revealed horizontal variability in these properties on meso- to micro scales which are relevant to phytoplankton dynamics. This variability increases dramatically in highly dynamic and

\*Correspondence: filipa.carvalho@noc.ac.uk

marine ecosystems, such as the coastal Southern Ocean (Lin et al. 2016). Although ship-based underway sampling was instrumental to document the variability and factors controlling photosynthetic rates in the near-surface layer, the use of underwater autonomous vehicles, such as gliders, provides an important practical tool to explore a high-resolution 3D structure of photosynthetic fluorescence properties in the water column. Airborne LIDAR fluorescence based techniques from planes and satellites can be used to overcome some of the gaps left by satellites, but data is limited on subsurface phytoplankton biomass (Churnside and Marchbanks 2015) or surface only photosynthetic characteristics (Chekalyuk et al. 2000).

Recent years have seen the rapid development of buoyancy-driven autonomous underwater vehicles (AUV) for oceanographic research (Griffiths et al. 2007). Some classes of the AUVs (buoyancy vehicles) can conduct sustained missions from weeks to a year (Schofield et al. 2007; Rudnick 2016) and are capable of carrying a wide range of sensors (Schofield et al. 2015). Here we report on the development of a variable fluorescence sensor for an autonomous buoyancy vehicle offering the potential for collecting phytoplankton photo-physiology data remotely, in situ, under ambient light with high spatial and temporal resolution. This technology was demonstrated during a series of deployments (Haskins and Schofield 2015; Carvalho et al. 2016a) in the coastal waters off the West Antarctica Peninsula, a region which is experiencing a rapid environmental change (Schofield et al. 2010).

Integrating a FIRE sensor on a glider provides sampling advantages over ships. These include: (1) Gliders allow sampling at the very near surface where ships (especially large ones) have difficulty sampling. Thus gliders have the ability to measure the physiology of a natural population that can be used to ground-truth algorithms developed to evaluate phytoplankton physiology from space. (2) The small footprint of a glider allows the collection of data without the ship-shadow effect that is significant when collecting shipboard measurements using instruments on a wire. (3) Gliders can be used in a semi-Lagrangian, water mass tracking mode to evaluate in situ physiological response (e.g., photoacclimation) of a phytoplankton community to local physical forcing, such as a gradual or abrupt deepening of the mixed layer, and provides a relatively cheap and reliable way to follow a water mass, collecting physical and biogeochemical properties over time in the same population. Pairing these data with turbulence measurements (which gliders are also capable of collecting) allow further evaluation at microscales. (4) Sustained spatial physiological observations for long periods is cost-effective for gliders. Given the proven reliability of gliders to provide sustained observations for months at a time, a FIRE on a glider would allow the collection of 3D maps of phytoplankton physiology across different scales (time and space) allowing us to assess the physical drivers of phytoplankton physiology over meso- and micro-scales.

This work showcases the FIRE glider as a new tool that will complement shipboard phytoplankton physiological measurements. It highlights some of the advantages and capabilities of miniaturizing and integrating an already established FIRE sensor on an autonomous platform. We characterize the instrument by running a series of comparisons to a benchtop mini-FIRE instrument and present some field demonstration deployments in the West Antarctic Peninsula. Finally, we describe and suggest a series of best practices when deploying this instrument on the field.

## Materials and procedures

### Autonomous platform

Teledyne Webb Research (TWR) Slocum electric gliders are a robust AUV platform capable of mapping properties within the upper water column (Schofield et al. 2007) that are increasingly filling mesoscale sampling needs for ocean science. Gliders maneuver across the ocean at a forward speed of 20–30 cm s<sup>-1</sup> in a triangle-shaped diving trajectory, deriving its forward propulsion by means of a buoyancy change and steering by means of a tail fin rudder. Pitch is regulated by shifting batteries back and forth within the glider. A depth sensor enables pre-programmed sampling of depth ranging from a minimum ~2–3 m (about 10 for deep gliders) to 1000 m on the downcast or on multiple successive dives without surfacing. On single dives, and especially on the upcast, Slocum gliders are capable of sampling all the way to the surface. Sensors carried by the gliders continuously record data during the glider descents/ascents, and a typical mission can collect thousands of vertical profiles. This allows the glider to collect high-resolution data in both time and space. Another great advantage of gliders over ships is the ability to sample both in Lagrangian or Eulerian mode, on demand. The glider can be set in drift mode, following this way the same water mass and record changes over the same population or operate virtual mooring (Clark et al. 2020), where the glider station keeps at one location (see Section “*Field evaluation and applications*” for specifically designed missions for the FIRE glider).

### Integrating variable fluorescence measurements into a glider

Bio-optical measurements of photosynthetic rates and physiological characteristics of phytoplankton are based on the use of variable fluorescence techniques (Huot and Babin 2010), including the FIRE technique (Gorbunov and Falkowski 2005). FIRE measurements are sensitive, fast, non-destructive, and can be performed in real-time (Gorbunov et al. 2020). The parameters (Table 1) derived from Kolber et al. (1998), are used to quantify the phytoplankton-specific photosynthetic performance in natural assemblages in aquatic ecosystems (Dubinsky and Schofield 2009) and provide a background for modeling the rates of primary production in the water column (Hughes et al. 2018; Ko et al. 2019).

**Table 1.** Notation of FIRE variables. See Cosgrove and Borowitzka (2010) for more details and synonyms.

Abr.	Description	Abr.	Description
$\sigma_{\text{PSII}}$	Functional absorption cross section of PSII in a dark-adapted state ( $\text{\AA}^2$ )	$\sigma_{\text{PSII}}'$	Functional absorption cross section of PSII in a light-adapted state ( $\text{\AA}^2$ )
$F_o, F_m$	Minimum and maximum yields of Chl <i>a</i> fluorescence (arbitrary units)	$F_o', F', F_m'$	Minimum, steady-state, and maximum of Chl <i>a</i> fluorescence measured under ambient light (arbitrary units)
$F_v$	Variable fluorescence, $F_m - F_o$	$F_v'$	Variable fluorescence measured under ambient light, $F_m' - F_o'$
$F_v/F_m$	Maximum quantum yield of photochemistry in PSII, measured in a dark-adapted state (dimensionless)	$\Delta F'/F_m'$	Quantum yield of photochemistry in PSII, measured under ambient light, $F_m' - F'/F_m'$ (dimensionless)
$E_k$	Light-saturation parameter ( $\mu\text{mol quanta m}^{-2} \text{s}^{-1}$ )	$\Delta F'$	Change in the fluorescence yield measured under ambient light, $F_m' - F'$
'	Prime indicates that measurements are collected under ambient light	$\Delta F'/F_v'$	Coefficient of photochemical quenching characterizing the fraction of open reaction centres in a light-adapted state

Fluorescence signals are excited by flashes from 450 nm light emitting diodes (LEDs), isolated by a 680 nm interference filter and detected by a sensitive avalanche photodiode module (Gorbunov and Falkowski 2005). The computer-controlled LED driver delivers pulses with varied duration from 0.5  $\mu\text{s}$  to 50 ms, which ensures fast saturation of PSII within a single photosynthetic turnover (STF, < 100  $\mu\text{s}$ ). In partnership with Teledyne Webb Research and Satlantic, a FIRE sensor was miniaturized and integrated into the Slocum glider science payload bay (Fig. 1), from now on referred to as a FIRE glider. Merging these two platforms allows for high-resolution

continuous and vertically resolved mapping of phytoplankton physiological parameters in the water column. This prototype was integrated into a Slocum G1 glider, a “shallow glider” rated for 100 m. Given the slow speeds of a glider, during the STF protocol, the glider only moves about 0.02–0.03 mm, so it is a fair assumption to consider the excitation constrained to a fixed sample in space relative to the detector, so no artifacts should be introduced by this moving platform, as long as only parameters from the 100  $\mu\text{s}$  burst are being used in the analyses.

### Other sensors

A photosynthetically active radiation (PAR) sensor is also incorporated in the FIRE science bay and is critical to the interpretation of the FIRE data. The standard Seabird Conductivity–Temperature–Depth (CTD) package in all gliders allows a high-resolution characterization of the physical setting, which provides critical data to relate physiological patterns associated with water column stability and mixed layer depth (Carvalho et al. 2017). The FIRE bay can be paired with an optional second science bay carrying a WET Labs Environmental Characterization Optics (ECO) pucks, measuring chlorophyll fluorescence, backscatter at several wavelengths, and/or colored dissolved organic matter (CDOM) fluorescence. Given the modular nature of Slocum gliders, other sensor pairings may be available on a second science bay or an extra stack-on bay, including extra energy bay to extend the deployment duration.

### Assessment and discussion

#### Laboratory evaluation

Silsbe et al. (2015) highlights the importance of calibrations and understanding sensor behavior given the inherent

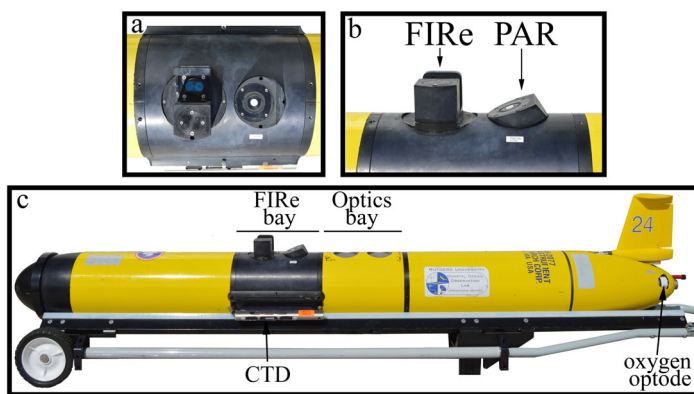


**Fig. 1.** Top (a) and side (b) view of the Fluorescence Induction and Relaxation (FIRE) and photosynthetic active radiation (PAR) sensors integrated into a Slocum glider FIRE bay (black section). (c) Extended Slocum glider with double science bay configuration with FIRE bay in front and optics bay with Seabird WET Labs ECO puck (measuring chlorophyll fluorescence, backscatter and/or colored dissolved organic matter), Seabird conductivity-temperature depth (CTD) sensor and Aanderaa dissolved oxygen optode in the aft. The glider is shown without its two lateral wings that connect to the black FIRE bay.

variability within instruments. Bench testing was conducted to characterize this instrument and to understand how it compares to conventional benchtop instrument, i.e., mini-FIRE. We: (1) evaluated the relationship between the maximum fluorescence,  $F_m$ , and standard measurements of extracted chlorophyll concentration; (2) evaluated the effect of incident light on the measurement sensitivity and signal-to-noise; (3) characterized pure water, filtered seawater and deep in situ blanks; and (4) characterized instrument behavior in pure water.

### Reference profile calibration

Like the bench-top FIRE instrument, the FIRE glider sensor requires a reference excitation profile, which is used to normalize the collected fluorescence intensities and to deduce fluorescence yields. This reference profile is acquired using a fluorescent dye (Rose Bengal) and is saved as a reference file. The reference profile reflects the actual shape of excitation intensity and has no variable fluorescence component. When processing the data collected during the deployment, the FIRE processing program will use this profile to calculate fluorescence yields. Given the high stability (< 0.5%) of this reference profile, due to the extremely stable and reproducible LEDs source, it is recommended the reference profile to be updated every 6 to 12 months.

### Relationship between FIRE $F_m$ and chlorophyll concentration

Like any fluorometer, the FIRE glider records fluorescence yields in arbitrary units. For these data to be used to assess phytoplankton biomass, maximum fluorescence yield ( $F_m$ ) needs to be calibrated against standard extracted measurements of chlorophyll concentration ( $\text{mg m}^{-3}$ ), to provide a proxy for phytoplankton biomass. These samples should be collected when and where the glider is being deployed as chlorophyll fluorescence yields may vary with community compositions.

Discrete samples were collected and evaluated in the (1) FIRE desktop, followed by the (2) FIRE glider, and finally (3) chlorophyll concentrations was estimated by filtering samples onto 25 mm Whatman GF/F filter and pigments extracted using 90% acetone, following the fluorometric method for phytoplankton chlorophyll determination (Yentsch and Menzel 1963). The filtered sample was then run again on both FIRE systems to evaluate blanks. A set of dilution experiments were conducted using water samples collected a few miles off Atlantic City (red, Fig. 2a,b) to increase the number of points and dynamic range in the  $F_m$  to chlorophyll concentration regression. Two sets of water sample calibrations from field deployments in the West Antarctic Peninsula were included in this analysis to add sample points with potentially different community compositions.  $F_m$  is less susceptible to variations in phytoplankton physiological state than  $F_o$  thus providing the best proxy for chlorophyll concentration. Comparison

between FIRE glider measured  $F_m$  and chlorophyll concentrations is shown in Fig. 2a. Correlation between the two variables was evaluated using a Model-II geometric mean linear regression  $y = 5.81x (5.44, 6.17) - 0.07 (-1.21, 1.06)$ ;  $r^2 = 0.98$ ;  $N = 43$ ).

To further characterize the custom-made glider integrated FIRE sensor, we ran the same discrete samples, in parallel, on the benchtop mini-FIRE, with filtered seawater (FSW) blank corrections applied for each system. To evaluate the correlation between  $F_v/F_m$  measured in each instrument, a model-2 major axis linear regression  $y = 1.07 (0.90, 1.24) - 0.10 (-0.22, 0.02)$ ,  $r^2 = 0.92$  was calculated. Given that the order of the individual replicates in each system is not correlated (3 per sample in each system), only sample averages were used in this analysis. Nevertheless, standard errors are shown in error bars in Fig. 2c. Some of the variability may reflect that the FIRE system on the glider is significantly older than mini-FIRE which has been developed more recently, where increased sensitivity is due to the improvement of electronic circuitries and the use of a more sensitive detector (Gorbunov et al. 2020).

### Blank correction

A “blank” is the background signal recorded from the sample, i.e., the signal associated with the absence of the property being studied, in this case, without chlorophyll fluorescence. In clear waters, the importance of blank collections has been highlighted (Cullen and Davis 2003; Bibby et al. 2008; Laney and Letelier 2008) because of fluorescence from dissolved organic matter (DOM) and phytoplankton degradation products (Benner and Strom 1993). In some instruments, electronic artifacts (Laney et al. 2001) and the effect of scatter by water itself (Laney et al. 2001) can present problems. The contribution of the latter two factors can be eliminated by improving the electronic and optical design. Although the magnitude and variability of the “blank” is usually small compared to chlorophyll fluorescence signals from phytoplankton in FIRE systems (Bibby et al. 2008), blanks should be routinely collected and subtracted from the fluorescence signals. However, in DOM-rich, low chlorophyll waters the blank correction may become critical for accurate retrievals of photosynthetic parameters (Bibby et al. 2008).

DI water blanks collected using this FIRE sensor integrated on the glider were overall very small ( $\text{blank}_{\text{DI water}} = 39 \pm 3.4$ , standard error), compared to the average chlorophyll fluorescence signal, corresponding to less than 3% of the lowest fluorescence recorded for a sample (i.e.,  $F_m = 1200 \text{ a.u.}$ ). Furthermore, the amount of incident light did not affect the signal when exposing the DI water at varying irradiances. The “standard” blanks using filtered seawater (FSW) were collected to evaluate the effect of dissolved organic matter in the recorded fluorescence signal. Apart from the two lowest concentrations tested (chlorophyll concentration <  $0.5 \text{ mg m}^{-3}$ ),

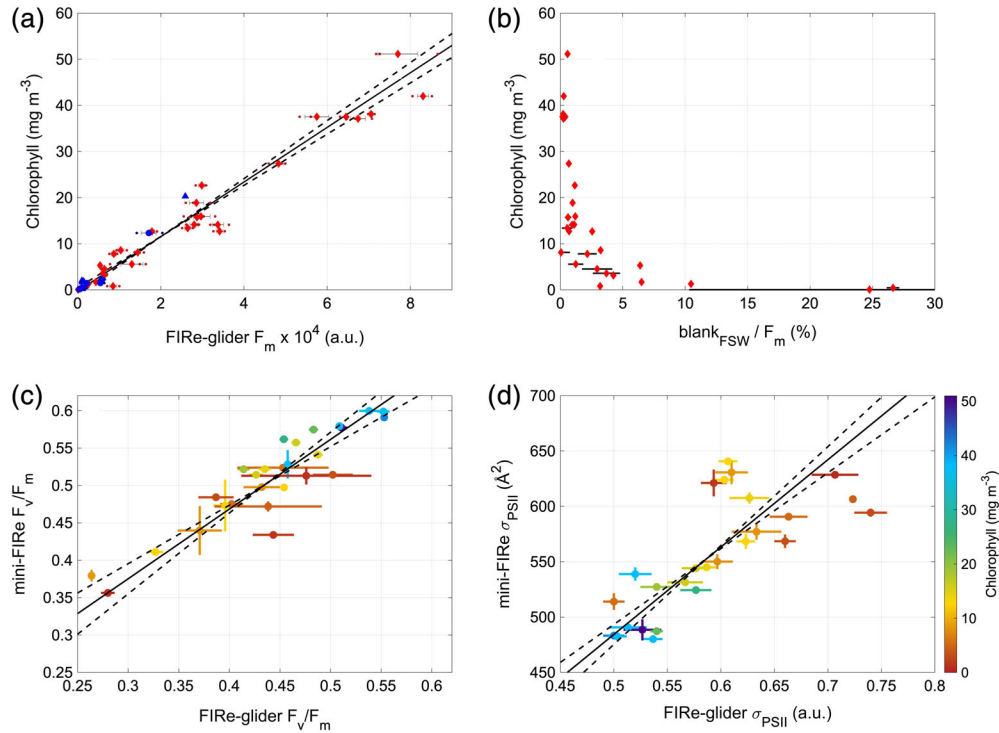


**Fig. 2.** Instrument calibration and characterization based on cross-comparison with the benchtop mini-FIRE instrument and discrete samples. **(a)** Relationship between maximum fluorescence ( $F_m'$  measured by the FIRE glider) and extracted chlorophyll concentration from in situ discrete samples. Different colors indicate different locations where water samples were collected (blue: West Antarctic Peninsula; red: New Jersey coastal waters). Individual measurements are shown in small colored dots, with averages shown in the large marker and standard errors for  $F_m$  in the horizontal bars. Model-II linear relationship ( $r^2 = 0.98$ ) and slope uncertainty (2 standard errors) are shown in solid and dashed lines, respectively. Triple FIRE replicates were used individually against a single chlorophyll concentration from that sample ( $N = 43$ ) for the regression analysis. **(b)** Ratio of freshwater (FSW) blank signal to  $F_m$ , against in situ chlorophyll concentration. Standard errors are shown in horizontal error bars. **(c)** Comparison of photosynthetic efficiency ( $F_v/F_m$ ) measured using the mini-FIRE and the FIRE-glider. Model-II linear regression ( $r^2 = 0.92$ ) and slope uncertainty (2 standard errors) of sample averages ( $N = 29$ ) are shown in solid and dashed lines, respectively. Error bars indicate standard errors shown for each sample measured in each instrument and are colored based on chlorophyll concentration. **(d)** Cross-calibration of the functional absorption cross-section ( $\sigma_{\text{PSII}}$ ). Comparison of sample averages (3 replicates each) between the FIRE-glider and the mini-FIRE with standard error bars for both instruments. Model-II linear regression ( $r^2 = 0.77$ ) and 2 standard errors of the slope uncertainty shown in solid and dashed lines.

the magnitude of the fluorescence of the blank normalized to the  $F_m$  was less than 5% for average chlorophyll concentration found in the upper ocean (Fig. 2b).

While it is impossible to measure appropriate in situ blanks concurrently with the FIRE glider measurements during deployment, in situ discrete water samples should be collected and analyzed in the lab bench before and after deployment. This will allow the evaluation of region-specific blanks as well as potential effect of biofouling during long deployments. No significant signs of biofouling were found after up to 3-week long deployments in coastal Antarctica, even though the instrument does not use any anti-biofouling technology such as copper plating. Although biofouling itself is unavoidable during long-term deployments, the impact of biofouling on the measured signals is dramatically reduced by the improved optical design of the glider FIRE sensor. The optical design employs a two-window configuration, which includes excitation and emission windows. Thereby, the collimated excitation light does not reach the emission optical window and

thus does not induce background fluorescence from biofouling material accumulated on this window. At the same time, fluorescence from biofouling accumulated on the excitation window does not reach the detector.

In all glider deployments conducted using the FIRE integration in coastal Antarctica, blanks corresponded to less than 1% of the chlorophyll fluorescence signal. Deep blanks, i.e., average signal in deep waters where we expect to find no phytoplankton, have been previously used when there is no chance to collect discrete in situ blanks. Using data from the field deployments, we found that the average “blank” signal at depth was higher ( $\sim 450$  a.u.) than the discrete blanks ran in the lab ( $\sim 330$  a.u.), likely due to the shallow profiling (100 m), constrained by the depth rating of the glider where this sensor was fitted to.

#### Functional absorption cross-section calibration

The functional absorption cross-section of Photosystem II ( $\sigma_{\text{PSII}}$ ) is a product of the optical absorption cross section of



PSII (i.e., the size of the PSII antennae) and the quantum yield of photochemistry in PSII (Falkowski et al. 2004). This biophysical parameter is controlled by photoacclimation status and nutrient availability, as well as affected by the community composition (Suggett et al. 2009).  $\sigma_{\text{PSII}}$  is calculated from the rate of fluorescence rise during the single turnover flash (STF), as this rate is proportional to the product of  $\sigma_{\text{PSII}}$  and the excitation intensity (Gorbunov and Falkowski 2005). Accurate calibration of the excitation intensity within the sounding volume of the FIRE sensor is critical for retrievals of  $\sigma_{\text{PSII}}$  in absolute units, Angstrom squared ( $\text{\AA}^2$ ). Such calibration is conducted as part of the standard calibration procedure of the FIRE sensor. Because the spatial distribution of excitation intensity in the sounding volume of the underwater glider FIRE sensor is less uniform than that in the benchtop instrument, the benchtop instrument is much easier and more accurate to be calibrated. To convert the measured  $\sigma_{\text{PSII}}$ , collected in relative units, into absolute units, angstrom squared ( $\text{\AA}^2$ ), a correction coefficient must be determined by cross-calibrating the FIRE glider sensor against a “standard” calibrated benchtop FIRE instrument. A model-II linear regression  $y = 789.2x$  ( $581.02, 997.45$ ) +  $89.66$  ( $-33.25, 212.56$ ) was calculated, with  $r^2 = 0.77$  (Fig. 2d).

### Field evaluation and applications

The FIRE glider capabilities were evaluated in the field by three coastal deployments off the West Antarctic Peninsula (Fig. 5), in Palmer Deep Canyon (Carvalho et al. 2016b) near Palmer Station. The following sub-sections demonstrate some of the applications of such integration, some field experiments and some operational recommendations.

#### Non-Photochemical quenching (NPQ)

One of the biggest advantages of the FIRE integration on a glider is the ability to make measurements under ambient light. Daytime profiles reflect the physiological status resulting from high light during peak irradiance hours while night-time profiles can be used as a dark-adapted state. While capturing a “true” dark-adapted state is usually a problem in many FRRf studies, the sampling under ambient light by the FIRE glider allows the evaluation of the gradual relaxation of NPQ, but also understand when the true reversal of the daytime inactivation caused by supra-optimal irradiances. The physiological characteristics available under these two conditions are presented in Fig. 3 and described in Table 1.

In this situation, nutrient stress can be assessed using night-time profiles only and both Non-Photochemical Quenching (NPQ), a physiological mechanism to protect the photosynthetic apparatus from photodamage, where excess energy is dissipated as heat (Muller et al. 2001; Milligan et al. 2012) and Photochemical Quenching (PQ) can be evaluated throughout the deployment. The NPQ parameter (Bilger and Bjorkman 1990) gives a straightforward estimate of the

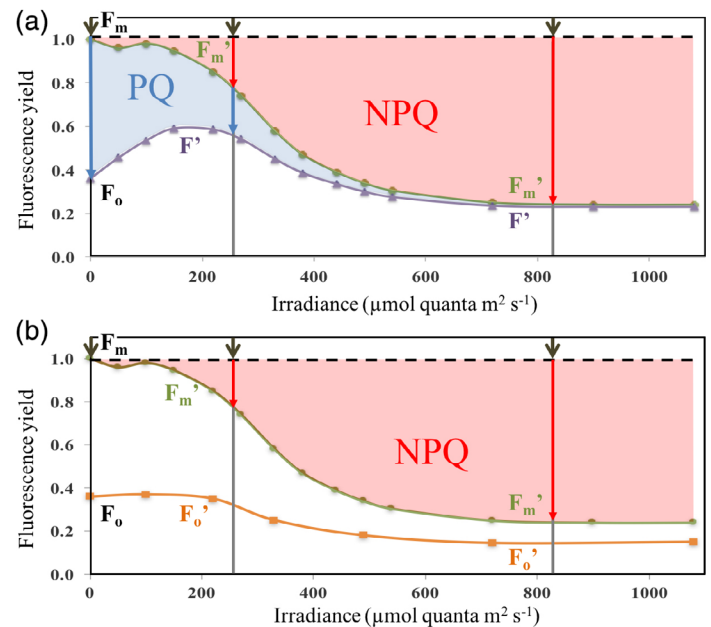


**Fig. 3.** Schematic of irradiance dependence of chlorophyll fluorescence yields. Measurements in: (a) light-adapted state, i.e., during daytime and (b) dark-adapted state, i.e., during night time.  $F_0$  and  $F_m$  are minimum (open reaction centres) and maximum (closed reaction centres) fluorescence yields measured in dark-adapted cells.  $F_0'$  and  $F_m'$  are the minimum and maximum fluorescence yields in a light adapted state.  $F$  is the actual fluorescence yield measured under ambient light. PQ and NPQ are photochemical quenching and non-photochemical quenching, respectively. Top gray arrows indicate example irradiances and its corresponding fraction of NPQ and PQ.

portion of thermally dissipated photon flux (i.e., the quantum yield of nonphotochemical quenching).

To determine  $F_m$  we can use the night-time profile where  $F_m'$  is maximal (finding the maximum  $F_m'$  between 22:00 and 6:00) the night immediately before or after the daytime period being considered. This relies on the assumption that the glider has not moved into a different water mass, which is more valid when sampling in a Lagrangian way, which gliders are capable of. A specific semi-Lagrangian mission designed for the FIRE glider is further detailed in section “Evaluate the physiological responses of the same phytoplankton community to changes in water column dynamics”.

The high resolution capability of gliders allows not only the timeseries analysis of NPQ at a particular depth (Fig. 4, left panels, in this case at 8 m depth), but also the characterization of a depth-resolved NPQ (Fig. 4, middle and right), important in situations where potentially different physiological communities react differently to varying irradiance. The two quenching components, non-photochemical quenching component (qN) and photochemical quenching component (qP), are defined in Kooten and Snel (1990). While the data is lacking in the upper 5-7 m for this example due to the deployment setup, the glider does have the capability to sample this

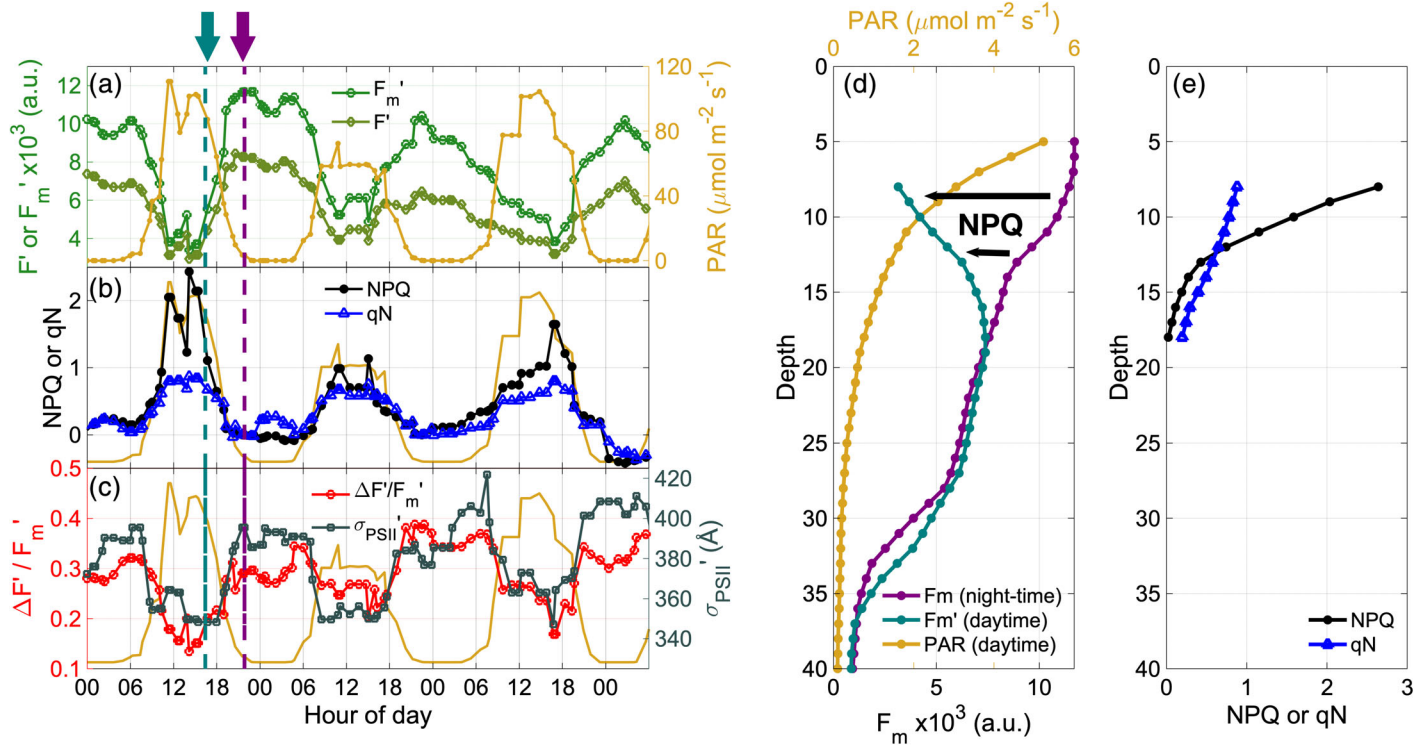


**Fig. 4.** Three diel cycles from a coastal deployment off the West Antarctic peninsula at 8 m depth of (a) fluorescence at steady-state ( $F'$ , light green) and maximum ( $F_m'$ , dark green) levels with factory calibrated photosynthetic active radiation (PAR, gold), (b) non-photochemical quenching (NPQ, black) and NPQ component (qN, blue); (c) the quantum yield of photochemistry in PSII ( $\Delta F'/F_m'$ , red) and functional absorption cross section for PSII ( $\sigma_{\text{PSII}}$ , gray). Vertical panels represent depth profiles of (d)  $F_m'$  during night-time (purple), determined by the maximum night-time fluorescence between 22:00 and 06:00 and a  $F_m'$  daytime example (teal) and (e) respective NPQ and qN.

layer and better inform the fluorescence kinetics where irradiance is highest.

#### Performance under low phytoplankton biomass conditions

Data collected over three different deployments in the West Antarctic Peninsula was used to evaluate the sensor sensitivity as a function of chlorophyll. Maximum fluorescence ( $F_m'$ ) was converted to chlorophyll using in situ discrete samples collected before and after deployments. For lower values of chlorophyll, there was more scatter, predominantly toward the negative values in  $F_v/F_m$  as, under low biomass (i.e., low signal-to-noise ratio), it gets increasingly difficult to distinguish first  $F_o$ , then  $F_m$ , from zero. Under low chlorophyll concentrations, poor fits of the biophysical model to the data were observed during the processing using the supplied Satlantic/Seabird software, resulting in still accurate  $F_m$  values (as shown by the good  $F_m$ :chl regression fit in Fig. 2a), but less certain estimates of  $F_o$ , where in most cases,  $F_o$  becomes negative. We will further on refer to these as “bad points,” but note that it is due to the poor model fit and not bad data collected. To further assess the minimum chlorophyll concentration in which we can accurately collect physiological data, bad points (7% of the data, of a total of 41,445 data points) were identified when

$F_v/F_m < 0$  (i.e.,  $F_o$  was either higher than  $F_m$  or negative) or  $F_v/F_m$  was higher than is commonly found in natural populations ( $F_v/F_m > 0.66$ ). Theoretically,  $F_o$  cannot be higher than  $F_m$  as in the scenario where the reaction centres are fully closed,  $F_o$  would equal  $F_m$ . Most “bad points” corresponded to  $F_v/F_m < 0$  (94%, matching low chlorophyll concentrations), while only a very small percentage corresponded to  $F_v/F_m > 0.66$  (6%). Fewer points in the scatter cloud were collected under high irradiance, with the majority being found below 50 m, under low light and where the signal-to-noise ratio was low. Applying a simple 3-point median filter to remove spikes resulted in a decrease of the “bad points” to 3.6% where a higher percentage (98.7%) corresponded to  $F_v/F_m < 0$ . Minimum chlorophyll concentration was calculated assuming different percentages of acceptable “bad points”: when considering 10% “bad points” acceptable using untreated/raw data (data with median filter applied in parenthesis), minimum chlorophyll concentration is 0.26 (0.23)  $\text{mg m}^{-3}$ , while for 5 and 1% are 0.32 (0.26) and 0.44 (0.38)  $\text{mg m}^{-3}$ , respectively, with results improving with a larger window on the median filter. While these results could be indicative of low sensitivity of the instrument, after a careful visual analysis of the output of the fitting software under low concentrations, we believe the increasing number of bad

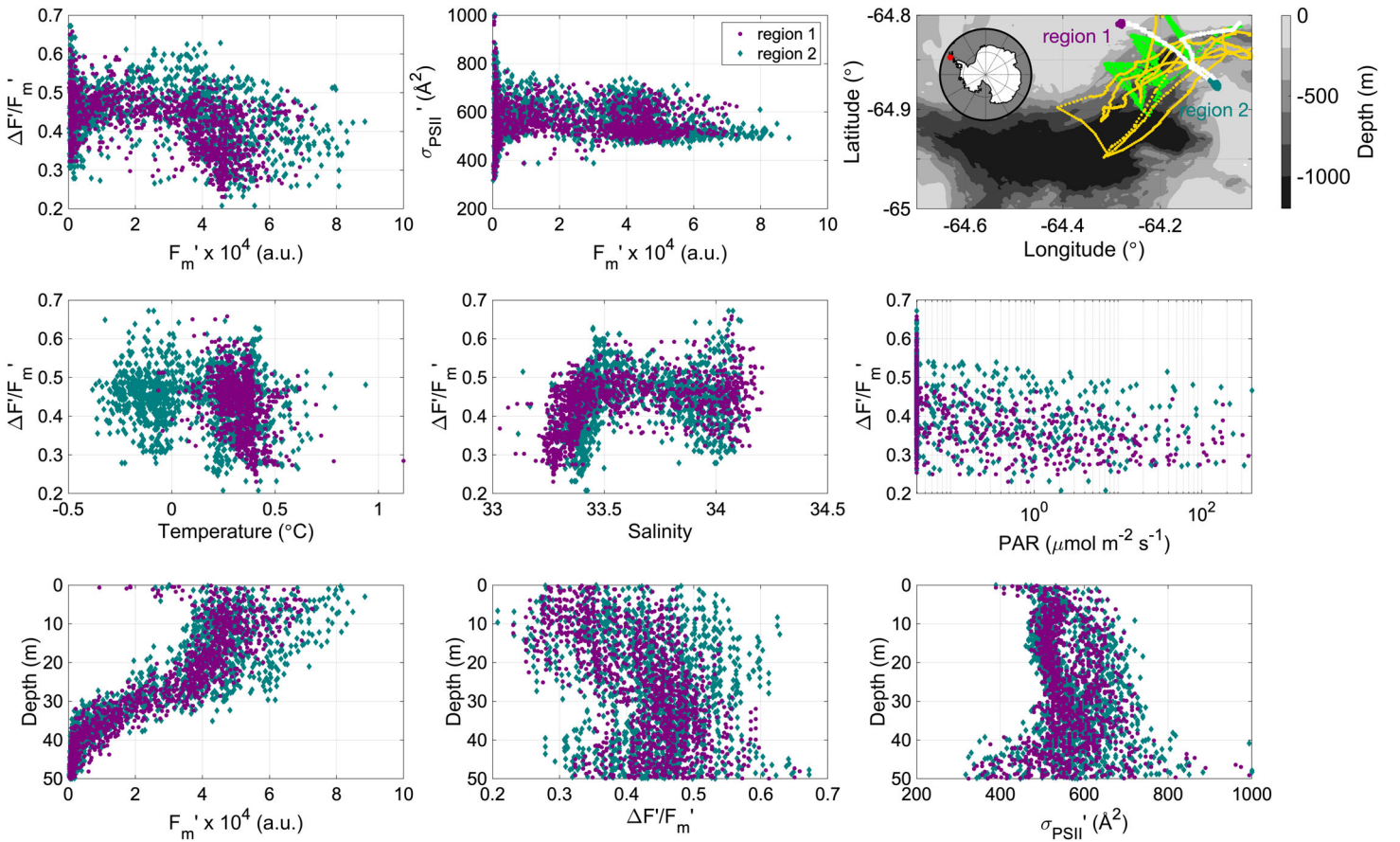


**Fig. 5.** Location of the three coastal deployments off the West Antarctic Peninsula shown in this manuscript, illustrating the station keeping mission (white, purple and teal for transit, region 1 and region 2, respectively), drift mission (yellow) and a zigzag mission (green). Scatter plots from the station keeping mission from Fig. 6 with the two diel cycles from each region showing different physiological responses to physical forcing: (top) Photosynthetic efficiency ( $\Delta F'/F'_m$ ) and functional absorption cross-section of PSII ( $\sigma_{PSII}'$ ) as a function of phytoplankton biomass ( $F'_m$ ); (middle)  $\Delta F'/F'_m$  as a functional of temperature, salinity, and PAR; (bottom) depth profiles of  $F'_m$ ,  $\Delta F'/F'_m$  and  $\sigma_{PSII}'$  for the two regions.

points at low concentrations are due to the poor curve fitting using the provided processing software. We believe this “sensitivity” can be further improved, if data is fitted manually (i.e., not using the provided software), as we found that misfits often resulted from just one potential outlier in the fluorescence induction curve. Unfortunately, the raw data files collected by the glider-integrated FIRE system are in a proprietary binary format which we were incapable of decoding, despite several unsuccessful attempts to interface with both Satlantic/Seabird, the commercial FIRE manufacturer, and Teledyne Webb Research, the glider manufacturer. Each file is individually processed on the software, where FIRE variables (Table 1) are derived; however, no statistics are reported for the quality fit of the biophysical model, so we are unable to fully characterize the robustness of the model fit. Given this constraint we were not able to demonstrate the reason for the poorer results low chlorophyll concentrations is not the instrument itself, instead it reflected issues with the proprietary software provided by Satlantic. Despite this problem, it represented only a

small proportion of the data (7% of the raw data) and future development efforts will be able to resolve this issue. However, given the high-resolution capabilities of the gliders, under low chlorophyll concentration, signal can be isolated from scatter/noise by averaging and using low-pass filters, as shown previously. The amount of data points from the glider would still surpass, by far, the ones collected manually, using discrete samples.

Two missions have been designed to evaluate physiological responses at different temporal and spatial scales: (1) compare and contrast physiological responses of phytoplankton to different physical forcing settings using Eulerian sampling (“station keeping mission”, white, purple and teal dots in the map from Fig. 5) and (2) evaluate the physiological responses of the same phytoplankton community to changes in water column dynamics (“drift mission”, yellow dots in the map from Fig. 5). A third mission was also conducted at the same location in a zigzag pattern (green dots in the map from Fig. 5) to increase the number of data points in the field assessment analyses.



**Compare and contrast physiological responses of phytoplankton to different physical forcing (“station keeping mission”)**

Often, the irradiance regime experienced by phytoplankton is a result of the complex interaction between incident irradiation, turbulent mixing and variations in the water column vertical structure (i.e., changes in the water column stability and MLD due to varying wind stress and water mass types as well as heat from insolation) (Neale et al. 2003). For a given temperature and nutrient status, phytoplankton regulate photosynthetic rates based on their light field by altering their photosynthetic apparatus. For example, the cellular chlorophyll content is usually higher when the cells have been growing under low light (Lewis et al. 1984; MacIntyre et al. 2000). It is then informative to analyze phytoplankton physiology in the context of their physical setting (Hughes et al. 2020).

The ability of the FIRE glider to collect, at high resolution, physiological data together with physical oceanographic parameters allows further analyses on the physical drivers of primary production. Gliders also offer an advantage compared to other oceanographic platforms in providing more flexibility in how, when and where they sample. It is sometimes beneficial to use gliders as virtual moorings when the scientific question involves a spatial comparison. An Eulerian approach allows data collection that isolates the temporal signal by removing space from the equation. Deploying the FIRE glider in station keeping (virtual mooring) mode in locations with different physical settings, one can infer how environmental variables are associated with phytoplankton physiology over time (Fig. 6). The degree with which the same population is being sampled depends on the local circulation. This mission was conducted in an area where physical and biological regional differences had been previously documented (Carvalho et al. 2016b; Kohut et al. 2018). Different water masses and degrees of stratification can be identified between the two regions (Figs. 5, 6), where overall higher  $\Delta F'/F_m'$ ,  $F_m'$  and  $\sigma_{PSII}'$  can be observed in region 2, an area with lower temperatures, increased PAR and higher salinity. Together with higher  $\Delta F'/F_m'$  across all PAR range, a clear diel signal is evident in  $\sigma_{PSII}'$  (showing high values during night-time and a decrease during daytime, Fig. 6). Ranges of measured  $\sigma_{PSII}'$  are shown in Figs. 5, 6 in accordance with previous studies (Behrenfeld and Kolber 1999; Suggett et al. 2009; Alderkamp et al. 2015).

**Evaluate the physiological responses of the same phytoplankton community to changes in water column dynamics (“drift mission”)**

The properties of phytoplankton community structure, such as cell size and taxonomy, influence photosynthetic rates and therefore variable fluorescence signals (Suggett et al. 2009). When evaluating the temporal pattern (e.g., diel cycles) in the photosynthetic efficiency of a phytoplankton community in situ, it is important to make sure that the measurements are

constrained to the same phytoplankton community. The best way to accomplish this in situ is to use a Lagrangian approach and follow the same water mass over time. While gliders are a platform capable of collecting a large amount of high-resolution profiles autonomously, one of its main constraints is the active movement into a potentially different water mass as they fly through the water column on their standard flight configuration. To stay within the same water mass and evaluate physiological changes of a phytoplankton community through time, a new mission was designed to avoid actively changing water masses. A glider cycle (“yo,” including a dive and a climb back to the surface) takes around 20 min. On this custom mission design, a “yo” was done every hour, where the rudder (steering) was set all the way to one side, resulting in a corkscrew dive and climb. The remaining time, in between the hourly dives, the glider would drift at the surface following the phytoplankton community present in the same water mass. This setup allows the collection of at least 24 profiles to characterize a diel cycle within the same water mass.

Stratification, mixed layer depth (MLD) and rates of vertical mixing have been identified as controls on primary production and phytoplankton dynamics (Lewis et al. 1984; Mitchell and Holm-Hansen 1991; MacIntyre et al. 2000). In a strongly mixed surface layer, phytoplankton acclimate to light levels averaged over the MLD (Lewis et al. 1984), so a relatively stable light environment as a result of a shallow MLD allows phytoplankton to photoacclimate on timescales of 1–2 d (Schofield et al. 1995). During intense mixing events, dim-light adapted phytoplankton may be brought toward the surface where they are exposed to supra-optimal irradiances, which leads to a decrease in both  $F_m'$  and  $\Delta F'/F_m'$ .

Photoadaptive parameters respond to changes in irradiance at different rates. Photoinhibition can be assessed in the fluorescence signal on time-scales of seconds to minutes while it takes several hours for the photosynthetic capacity to be compromised (Lewis et al. 1984). Effects of high irradiance periods (hours 10–16) shown by the yellow colors in the Photosynthetically Active Radiation (Fig. 7, bottom) are evident by the low values seen in the photosynthetic efficiency ( $\Delta F'/F_m'$ , Fig. 7) maximum fluorescence ( $F_m'$  or proxy for chlorophyll concentration (Fig. 7), and in the functional absorption cross-section ( $\sigma_{PSII}'$ , Fig. 7). This is evidence of NPQ, with the deepest penetration occurring during peak irradiance (hour 13–14). Increased fluorescence signal was found under shallower MLD. NPQ was more marked in the deeper MLD (lower  $F_m'$ , Fig. 7) regime where phytoplankton are acclimated to lower light. The collection of high-resolution photo-physiology parameters over a diel cycle permits the evaluation of NPQ under supra-irradiance as seen by a decrease in  $\Delta F'/F_m'$ ,  $F_m'$ , and  $\sigma_{PSII}'$ , as compared to their dark-adapted values.

Light-induced mechanisms used to prevent photodamage under high irradiance, such as NPQ, result in changes in the functional absorption cross-section of PSII ( $\sigma_{PSII}'$ ) (Krause and Weis 1991; Falkowski et al. 1994). This decrease in  $\sigma_{PSII}'$  can be

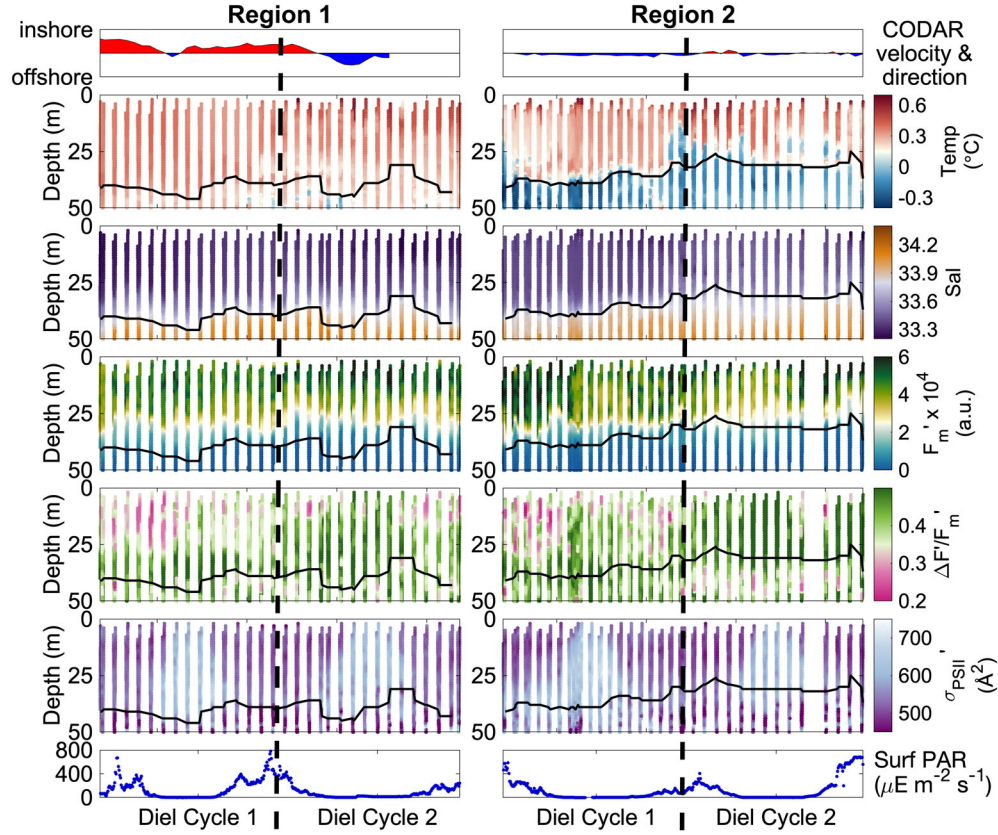


**Fig. 6.** Two diel cycles separated by the black vertical dotted line (as outlined in the surface PAR, bottom) collected in two regions with different oceanographic conditions. Direction and magnitude of the dominant surface currents (top, from HF radars) are in part responsible for changes in the vertical structure of the water column as demonstrated by the temperature and salinity panels and the depth of the mixed layer (black line). Remaining rows report FIR measurements— $F_m'$  (relative units),  $\Delta F'/F_m'$  (dimensionless) and  $\sigma_{PSII}'$  (functional absorption cross-section of PSII,  $\text{\AA}^2$ ). Adapted from Carvalho et al. (2016a).

close to 50%, implying a matching reduction in the excitation delivery to the reaction centres of Photosystem II and a shift of  $E_k$  to higher values as seen in left  $\sigma_{PSII}'$  panel in Fig. 7 and left panels in Fig. 8.

#### Photoacclimation mechanisms evaluation

To cope with high light-induced stresses (i.e., to optimize light absorption under low light conditions or even to reduce total photon utilization under supra-optimal irradiances) phytoplankton have developed a suite of photoadaptation mechanisms. Using the drift mission data, we can compare the different photoacclimation responses to MLD dynamics (e.g., shallow vs. deep mixed layer). When cells photoacclimate, they adjust their photosynthetic machinery to operate at the highest quantum yield possible that allows for the maximal rate of photosynthesis. This occurs at the inflection point in the photosynthesis irradiance curve, the light saturation parameter ( $E_k$ ) (Dubinsky and Schofield 2009). Bio-optical models (Webb et al. 1974; Jassby and Platt 1976) describe the relationship between photosynthesis and irradiance. The hyperbolic tangent model has become one of the most widely

used models for predicting photosynthetic rates in natural phytoplankton assemblages. The photosynthetic rates ( $P$ ) as a function of PAR are described by the following equation (Jassby and Platt 1976):

$$P = P_{\max} \left[ \tanh \left( \frac{\text{PAR}}{E_k} \right) \right] \quad (1)$$

where PAR is photosynthetically active radiation,  $P_{\max}$  is the maximum rate achieved at saturating light, and  $E_k$  is the light saturation parameter. The quantum yield ( $\Delta F'/F_m'$ ) is, by definition, proportional to the ratio of  $P$  to PAR:

$$\frac{\Delta F'}{F_m'} = c \frac{E_k}{\text{PAR}} \left[ \tanh \left( \frac{\text{PAR}}{E_k} \right) \right] \quad (2)$$

where  $\Delta F'/F_m'$  is the quantum yield of photochemistry in PSII, measured under ambient light and  $c$  is a constant that corresponds to  $F_v/F_m$  measured in a dark-adapted state at  $\text{PAR} = 0$ , essentially  $\alpha$  in a P-E curve. Changes in  $E_k$  values provide insight on photoacclimation regimes due to a combination of

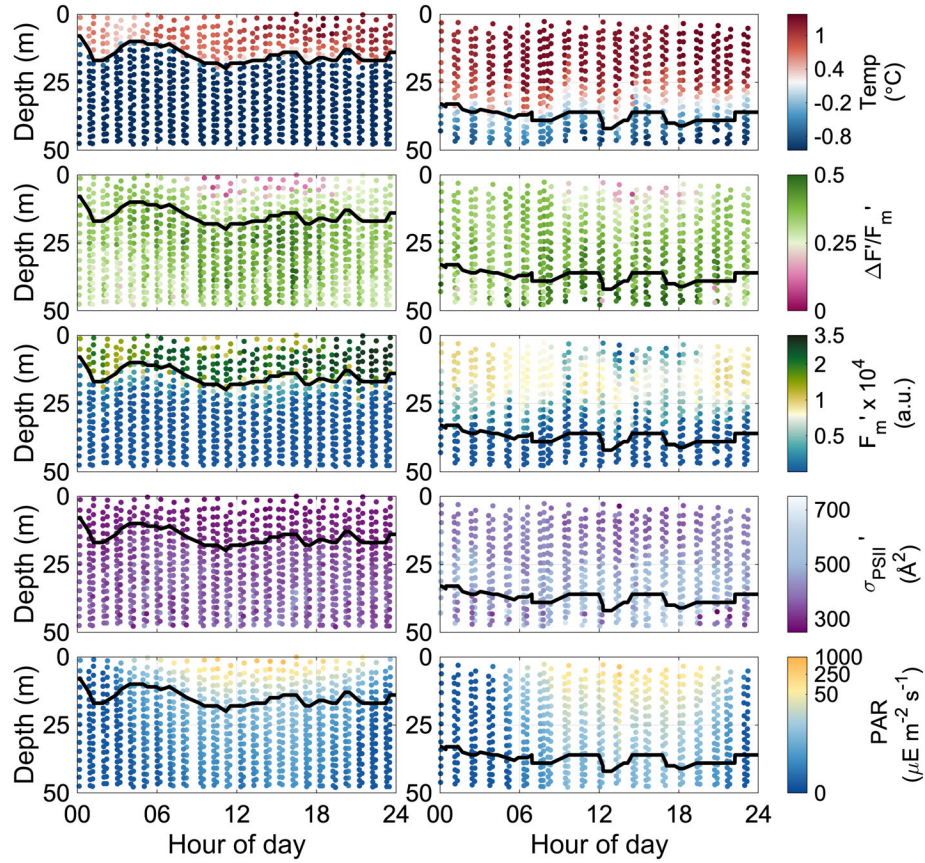


**Fig. 7.** Example of diel cycles collected during the drift mission for shallow (left panels) and deeper (right panels) mixing regimes. The depth of the mixed layer is shown with a black line. Gaps in data show times where glider was drifting at the surface. One profile was collected every hour. Effects of high irradiance periods (hours 10–16) shown in yellow in the Photosynthetically active radiation panels are evident by the low values seen in  $\Delta F'/F'_m$  (photosynthetic efficiency),  $F'_m$  (proxy for biomass) and  $\sigma_{PSII}$  (functional absorption cross-section). A warming of the upper ocean (temperature) is also seen during the highest irradiances. Adapted from Carvalho et al. (2016a).

the light field that phytoplankton are exposed and the mixing scales that can dominate the kinetics of primary productivity over the time-course of a day. This method can also be useful to evaluate the role of mixing in the competition between algal species (Falkowski and Woodhead 2013).

Applying this model (Eq. 2) to the high-resolution data from the FIRE glider during the drift mission we can estimate  $E_k$  and explain photoacclimatory responses of phytoplankton to changes in different MLD dynamics regimes (Figs. 7, 8).

Under a shallow MLD regime (Figs. 7, 8, left panel), where the light penetration reaches closer to the bottom of the ML, there is likelihood of two potential different physiological communities (i.e., communities with different photoacclimation regimes) as evaluated by the different  $E_k$  (compare orange and purple layers in Fig. 8). The much higher  $E_k$  seen at the surface gives an indication of phytoplankton acclimated to high irradiances while the lower  $E_k$  seen below the MLD shows lower light acclimation. Under deeper MLD conditions,  $E_k$  values are much closer (compare orange with purple box within the same MLD regime) indicating

photoacclimation is similar between the two layers (Fig. 8). These measurements and the derived depth dependent variability of the light saturation parameter are difficult to measure using standard ship-based sampling strategies and cannot provide sustained measurements over time. The glider approach allows for these processes to be directly measured under ambient light and data collected over the deployment allows the rates of photoacclimation for natural populations to be measured as the physical features, such as the mixed layer depth, evolve over time, which are important controls on primary production.

The current configuration of the glider FIRE prototype allows the collection of an average induction curve every 2.5–3 m. This vertical resolution is constrained by the maximum sampling rate and by fixed pitch flying due to the configuration of the PAR sensor. Only upcast data are used for accurate PAR measurements, since the mounted PAR sensor is upward looking angled at  $-20^\circ$  (Fig. 1). Multiple profiles are needed to increase the signal-to-noise ratio and provide a statistically significant fit to estimate  $E_k$ . For this dataset it required a

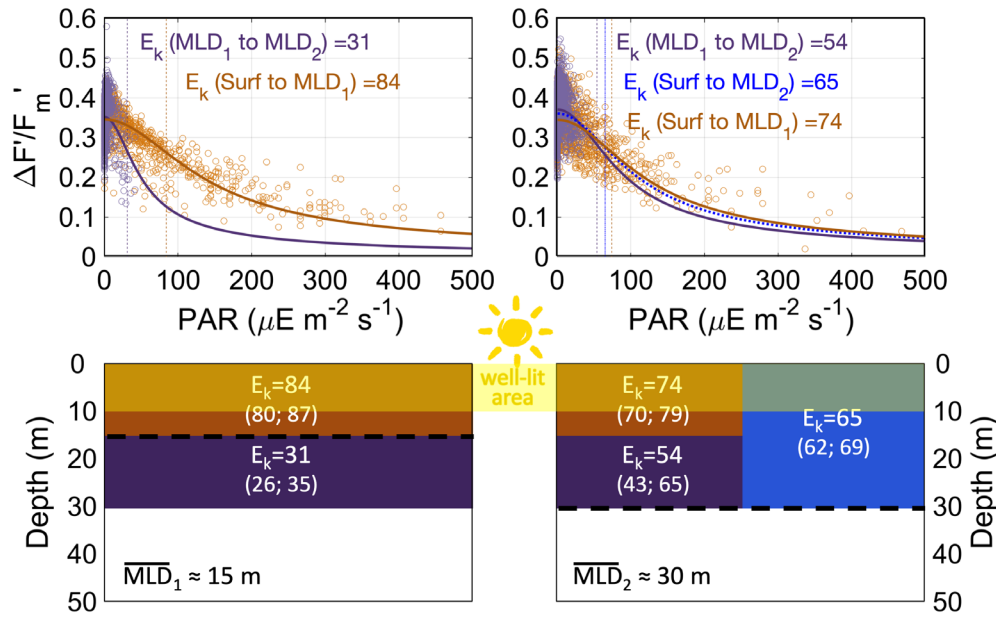


**Fig. 8.** (Top) Scatter plots of  $\Delta F'/F'_m$  and PAR with curve fits (Eq. 2) for the two MLD regimes collected during the drift mission shown on Fig. 7 (upcast data only), highlighting the effect of MLD on phytoplankton photoacclimation. (left) average MLD<sub>1</sub> is 15 m, i.e., shallower. (right) average MLD<sub>2</sub> is 30 m, i.e., deeper. Three depth bins (surface to MLD<sub>1</sub>—Orange, MLD<sub>1</sub> to MLD<sub>2</sub>—purple, and surface to MLD<sub>2</sub>—blue) were created to evaluate potential different phytoplankton photoacclimation regimes. Light saturation parameters,  $E_k$ , for each fitting are also presented. (bottom) Simple box model schematic with different depth bins, highlighting the different photoacclimation regimes presented in the plots on top, by comparing the  $E_k$  in each box, in relation to the MLD (black dashed line). Given PAR profiles from the glider, well-lit region of the upper ocean is shaded in yellow (top 10 m). 95% confidence intervals are presented in brackets for the  $E_k$  parameter estimation.

minimum of  $\sim 700$  points, which corresponds to  $\sim 20$  profiles using the current setup, all collected over a single diel cycle, to estimate a robust depth resolved  $E_k$  value. This number was obtained by evaluating the minimum number of points necessary to include in the analysis for the  $E_k$  to converge to a stable estimate.

### Operational recommendations

Note that power is probably the biggest constrain when fitting a FIRE sensor on a glider. The factory estimated power consumption of the sensor is 5.88 W, but field data shows power consumption closer to 5.5 W, depending on the sampling rate, whether the instrument is on all the time and other fitted sensors. From our field experience, a deployment with the FIRE integration, where the sensors are kept always on, lasts about 10 and 36 d, using an alkaline and a lithium primary battery pack, respectively. In practice, given that shallow gliders collect one profile every 10–15 min, a reduction in profile frequency can extend the deployment length and maximize data collection. Sampling just on the upcast (as downcasts lack FIRE data in the upper 6–8 m given the time needed for the instrument to turn on and given the positioning of the PAR sensor), or even every other upcast still provides 2–3 profiles every hour and can double the deployment length. Depending on the science focus, namely nutrient limitation studies, sampling only during night-time can make a

big difference in power consumption. Our planned station-keeping mission meant, contrary to the drift mission, that the glider is flying and collecting physical data continuously. A FIRE “yo” (upcast and downcast) every hour or so is a good compromise between the collection of high-resolution diel cycles of phytoplankton physiology and the mission longevity. Keep in mind, the ability to communicate with the glider means the duty cycle can be adjusted during the mission.

### Comments and recommendations

Underwater gliders have proven to be a robust technology for autonomous high-resolution collection of oceanographic data. The integration of a FIRE sensor in a Slocum glider allows the evaluation of phytoplankton physiology in relation to the physical conditions. It also has the additional advantage of collecting in situ data under ambient light. Such data is fundamental for modeling instantaneous rates of primary production and the water-column integrated primary production (Ko et al. 2019). Using variable chlorophyll fluorescence, physiological parameters can be used to assess environmental factors controlling phytoplankton productivity. Gliders offer an added sampling flexibility in terms of both steering and endurance, by providing an opportunity to design missions to target specific scientific goals such as assessing the progression of a phytoplankton population through time or evaluating



how different physical settings influence physiological responses. The high-resolution capabilities in both time and space permit the collection of diel cycles that allow a better understanding how phytoplankton react to variations in irradiance over different timescales.

Analysis of the irradiance dependencies of variable fluorescence signals provides insight into photoacclimation responses of phytoplankton to variations in vertical mixing regimes. While we realize that analyzing data from this FIRE sensor integration entails several assumptions and comes from a prototype, this study demonstrates the potential applications of this technology in autonomous platforms. Future plans include improving the sensor sensitivity to allow the use of the FIRE glider in oligotrophic regions. Increased flexibility to sample from different sensors independently from the FIRE sensor would be another helpful modification as it would allow extra data to be collected. The current integrated PAR sensor restricts the amount of data points collected during the profile as we cannot change the pitch to slow down the glider. Integrating a scalar irradiance PAR response would allow not only downcast sampling, but changing the pitch to slow the glider resulting in increased vertical resolution of photoacclimation parameters. Still, at a rate of  $\sim 0.4$  measurements per metre, in a single 2-week mission, 592 profiles of FIRE data were collected, including over 17,000 induction curves, which corresponds to about 30 points per 100 m profile.

Another improvement would be integration of an ultra-high sensitive multi-color FIRE sensor (Gorbunov et al. 2020) onto the glider that allows selective excitation of different functional groups of phytoplankton, spectrally resolved functional absorption cross-sections of PSII. Such an integration would offer the potential to enhance sampling resolution, as well as to monitor changes in taxonomic composition of phytoplankton communities.

## References

- Alderkamp, A., G. L. van Dijken, K. E. Lowry, and T. L. Connelly. 2015. Fe availability drives phytoplankton photosynthesis rates during spring bloom in the Amundsen Sea Polynya, Antarctica. *Elementa: Science of the Anthropocene*. **3**: 000043. doi: [10.12952/journal.elementa.000043](https://doi.org/10.12952/journal.elementa.000043)
- Behrenfeld, M. J., and Z. S. Kolber. 1999. Widespread iron limitation of phytoplankton in the south pacific ocean. *Science* **283**: 840–843. doi: [10.1126/science.283.5403.840](https://doi.org/10.1126/science.283.5403.840)
- Benner, R., and M. Strom. 1993. A critical evaluation of the analytical blank associated with DOC measurements by high-temperature catalytic oxidation. *Mar. Chem.* **41**: 153–160. doi: [10.1016/0304-4203\(93\)90113-3](https://doi.org/10.1016/0304-4203(93)90113-3)
- Bibby, T. S., M. Y. Gorbunov, K. W. Wyman, and P. G. Falkowski. 2008. Photosynthetic community responses to upwelling in mesoscale eddies in the subtropical North Atlantic and Pacific oceans. *Deep-Sea Res. II Top. Stud. Oceanogr.* **55**: 1310–1320. doi: [10.1016/j.dsr2.2008.01.014](https://doi.org/10.1016/j.dsr2.2008.01.014)
- Bilger, W., and O. Bjorkman. 1990. Role of the xanthophyll cycle in photoprotection elucidated by measurements of light-induced absorbance changes, fluorescence and photosynthesis in leaves of *Hedera canariensis*. *Photosynth. Res.* **25**: 173–185. doi: [10.1007/BF00033159](https://doi.org/10.1007/BF00033159)
- Carvalho, F., J. Kohut, M. Gorbunov, O. Schofield, and M. J. Oliver. 2016a. Mapping Antarctic phytoplankton physiology using autonomous gliders, p. 1–6. *In* Mapping Antarctic phytoplankton physiology using autonomous gliders. OCEANS 2016 MTS/IEEE Monterey. doi: [10.1109/OCEANS.2016.7761193](https://doi.org/10.1109/OCEANS.2016.7761193)
- Carvalho, F., J. Kohut, M. J. Oliver, and O. Schofield. 2017. Defining the ecologically relevant mixed-layer depth for Antarctica's coastal seas. *Geophys. Res. Lett.* **44**: 338–345. doi: [10.1002/2016gl071205](https://doi.org/10.1002/2016gl071205)
- Carvalho, F., J. Kohut, M. J. Oliver, R. M. Sherrell, and O. Schofield. 2016b. Mixing and phytoplankton dynamics in a submarine canyon in the West Antarctic peninsula. *J. Geophys. Res. Oceans* **121**: 5069–5083. doi: [10.1002/2016jc011650](https://doi.org/10.1002/2016jc011650)
- Chekalyuk, A., and M. Y. Gorbunov. 1993. Laser remote sensing of Phytoplankton Photosynthetic Activity In-Situ. *Int. Arch. Photogramm. Remote Sens.* **29**: 897–900.
- Chekalyuk, A. M., F. E. Hoge, C. W. Wright, R. N. Swift, and J. K. Yungel. 2000. Airborne test of laser pump-and-probe technique for assessment of phytoplankton photochemical characteristics. *Photosynth. Res.* **66**: 45–56. doi: [10.1023/A:1010764420934](https://doi.org/10.1023/A:1010764420934)
- Churnside, J. H., and R. D. Marchbanks. 2015. Subsurface plankton layers in the Arctic Ocean. *Geophys. Res. Lett.* **42**: 4896–4902. doi: [10.1002/2015gl064503](https://doi.org/10.1002/2015gl064503)
- Clark, E. B., and others. 2020. Station-keeping underwater gliders using a Predictive Ocean circulation model and applications to SWOT calibration and validation. *IEEE J. Oceanic Eng.* **45**: 371–384. doi: [10.1109/joe.2018.2886092](https://doi.org/10.1109/joe.2018.2886092)
- Cosgrove, J., and M. A. Borowitzka. 2010. Chlorophyll fluorescence terminology: An introduction, p. 1–17. *In* D. J. Suggett, O. Prášil, and M. A. Borowitzka [eds.], *Chlorophyll a fluorescence in aquatic sciences: Methods and applications*. Netherlands: Springer.
- Cullen, J. J., and R. F. Davis. 2003. The blank can make a big difference in oceanographic measurements. *Limnol. Oceanogr. Bull.* **12**(2): 29–35. doi: [10.1002/lob.200312229](https://doi.org/10.1002/lob.200312229)
- Dubinsky, Z., and O. Schofield. 2009. From the light to the darkness: Thriving at the light extremes in the oceans. *Hydrobiologia* **639**: 153–171. doi: [10.1007/s10750-009-0026-0](https://doi.org/10.1007/s10750-009-0026-0)
- Falkowski, P. G., R. M. Greene, and Z. Kolber. 1994. Light utilization and photoinhibition of photosynthesis in marine phytoplankton. *In* N. R. Baker and J. R. Bowyer [eds.], *Photoinhibition of Photosynthesis from Molecular Mechanisms to the Field*. Oxford: Bios Scientific Publishers. 409–434.

- Falkowski, P. G., and A. H. Knoll. 2007. An Introduction to Primary Producers in the Sea: Who They Are, What They Do, and When They Evolved. In P. G. Falkowski and A. H. Knoll [eds.], *Evolution of primary producers in the sea*, p. 1–6. Burlington, MA, USA: Elsevier Academic Press.
- Falkowski, P. G., M. Koblizek, M. Gorbunov, and Z. Kolber. 2004. Development and application of variable chlorophyll fluorescence techniques in marine ecosystems, p. 757–778. In *Chlorophyll a fluorescence*. Springer.
- Falkowski, P. G., and J. A. Raven. 2007. *Aquatic photosynthesis*. Princeton, NJ: Princeton University Press. 488.
- Falkowski, P. G., and A. D. Woodhead. 2013. *Primary productivity and biogeochemical cycles in the sea*. Boston, MA: Springer; 550. doi: [10.1007/978-1-4899-0762-2](https://doi.org/10.1007/978-1-4899-0762-2)
- Gorbunov, M. Y., and P. G. Falkowski. 2005. Fluorescence induction and relaxation (FIRE) technique and instrumentation for monitoring photosynthetic processes and primary production in aquatic ecosystems, p. 1029–1031. In A. van der Est and D. Bruce [eds.], *Photosynthesis: Fundamental Aspects to Global Perspectives—Proc. 13th International Congress of Photosynthesis*, Montreal, Aug 29 – Sep 3. Montreal: Allen Press.
- Gorbunov, M. Y., P. G. Falkowski, and Z. S. Kolber. 2000. Measurement of photosynthetic parameters in benthic organisms in situ using a SCUBA-based fast repetition rate fluorometer. *Limnol. Oceanogr.* **45**: 242–245. doi:[10.4319/lo.2000.45.1.0242](https://doi.org/10.4319/lo.2000.45.1.0242)
- Gorbunov, M. Y., Z. S. Kolber, M. P. Lesser, and P. G. Falkowski. 2001. Photosynthesis and photoprotection in symbiotic corals. *Limnol. Oceanogr.* **46**: 75–85. doi:[10.4319/lo.2000.45.1.0242](https://doi.org/10.4319/lo.2000.45.1.0242)
- Gorbunov, M. Y., E. Shirsin, E. Nikonova, V. V. Fadeev, and P. G. Falkowski. 2020. A multi-spectral fluorescence induction and relaxation (FIRE) technique for physiological and taxonomic analysis of phytoplankton communities. *Mar. Ecol. Prog. Ser.* **644**: 1–13. doi:[10.3354/meps13358](https://doi.org/10.3354/meps13358)
- Griffiths, G., C. Jones, J. Ferguson, and N. Bose. 2007. Under-sea gliders. *J. Ocean Technol.* **2**: 64–75.
- Haskins, C., and O. Schofield. 2015. Glider measurements of phytoplankton physiology in penguin foraging zones along the Western Antarctic Peninsula. In *OCEANS 2015—MTS/IEEE Washington*. doi: [10.23919/OCEANS.2015.7404376](https://doi.org/10.23919/OCEANS.2015.7404376)
- Hughes, D. J., and others. 2018. Roadmaps and detours: Active chlorophyll- a assessments of primary productivity across marine and freshwater systems. *Environ. Sci. Technol.* **52**: 12039–12054. doi:[10.1021/acs.est.8b03488](https://doi.org/10.1021/acs.est.8b03488)
- Hughes, D. J., J. R. Crosswell, M. A. Doblin, K. Oxborough, P. J. Ralph, D. Varkey, and D. J. Suggett. 2020. Dynamic variability of the phytoplankton electron requirement for carbon fixation in eastern Australian waters. *J. Mar. Syst.* **202**: 103252. doi:[10.1016/j.jmarsys.2019.103252](https://doi.org/10.1016/j.jmarsys.2019.103252)
- Huot, Y., and M. Babin. 2010. Overview of Fluorescence Protocols: Theory, Basic Concepts, and Practice, p. 31–74. In D. J. Suggett, O. Prášil, and M. A. Borowitzka [eds.], *Chlorophyll a fluorescence in aquatic sciences: Methods and applications*. Netherlands: Springer. doi:[10.1007/978-90-481-9268-7\\_3](https://doi.org/10.1007/978-90-481-9268-7_3)
- Jassby, A. D., and T. Platt. 1976. Mathematical formulation of the relationship between photosynthesis and light for phytoplankton. *Limnol. Oceanogr.* **21**: 540–547. doi:[10.4319/lo.1976.21.4.0540](https://doi.org/10.4319/lo.1976.21.4.0540)
- Ko, E., J. Park, M. Y. Gorbunov, and S. Yoo. 2019. Uncertainties in variable fluorescence and <sup>14</sup>C methods to estimate primary production: A case study in the coastal waters off the Korean peninsula. *Mar. Ecol. Prog. Ser.* **627**: 13–31. doi:[10.3354/meps13083](https://doi.org/10.3354/meps13083)
- Kohut, J. T., P. Winsor, H. Statscewich, M. J. Oliver, E. Fredj, N. Couto, K. Bernard, and W. Fraser. 2018. Variability in summer surface residence time within a West Antarctic peninsula biological hotspot. *Philos. Trans. R. Soc. A: Math. Phys. Eng. Sci.* **376**: 20170165. doi:[10.1098/rsta.2017.0165](https://doi.org/10.1098/rsta.2017.0165)
- Kolber, Z., O. Prášil, and P. G. Falkowski. 1998. Measurements of variable chlorophyll fluorescence using fast repetition rate techniques: Defining methodology and experimental protocols. *Biochim. Biophys. Acta (BBA)-Bioenergetics* **1367**: 88–106. doi:[10.1016/S0005-2728\(98\)00135-2](https://doi.org/10.1016/S0005-2728(98)00135-2)
- Kolber, Z., J. Zehr, and P. Falkowski. 1988. Effects of growth irradiance and nitrogen limitation on photosynthetic energy conversion in photosystem II. *Plant Physiol.* **88**: 923–929. doi:[10.1104/pp.88.3.923](https://doi.org/10.1104/pp.88.3.923)
- Kooten, O., and J. F. Snel. 1990. The use of chlorophyll fluorescence nomenclature in plant stress physiology. *Photosynth. Res.* **25**: 147–150. doi:[10.1007/BF00033156](https://doi.org/10.1007/BF00033156)
- Krause, G. H., and E. Weis. 1991. Chlorophyll fluorescence and photosynthesis: The basics. *Annu. Rev. Plant Phys.* **42**: 313–349. doi:[10.1146/annurev.pp.42.060191.001525](https://doi.org/10.1146/annurev.pp.42.060191.001525)
- Laney, S., R. Letelier, R. Desiderio, M. R. Abbott, D. Kiefer, and C. Booth. 2001. Measuring the natural fluorescence of phytoplankton cultures. *J. Atmos. Oceanic Tech.* **18**: 1924–1934. doi:[10.1175/1520-0426\(2001\)018<1924:MTNFOP>2.0.CO;2](https://doi.org/10.1175/1520-0426(2001)018<1924:MTNFOP>2.0.CO;2)
- Laney, S. R., and R. M. Letelier. 2008. Artifacts in measurements of chlorophyll fluorescence transients, with specific application to fast repetition rate fluorometry. *Limnol. Oceanogr.: Methods* **6**: 40–50. doi:[10.4319/lom.2008.6.40](https://doi.org/10.4319/lom.2008.6.40)
- Lewis, M. R., J. J. Cullen, and T. Platt. 1984. Relationships between vertical mixing and photoadaptation of phytoplankton: Similarity criteria. *Mar. Ecol. Prog. Ser.* **15**: 141–149. doi:[10.3354/meps015141](https://doi.org/10.3354/meps015141)
- Lin, H., F. I. Kuzminov, J. Park, S. Lee, P. G. Falkowski, and M. Y. Gorbunov. 2016. Phytoplankton. The fate of photons absorbed by phytoplankton in the global ocean. *Science* **351**: 264–267. doi:[10.1126/science.aab2213](https://doi.org/10.1126/science.aab2213)
- Lorenzen, C. J. 1966. A method for the continuous measurement of in vivo chlorophyll concentration. *Deep Sea Res. Oceanogr. Abstr.* **13**(2): 223–227. doi: [10.1016/0011-7471\(66\)91102-8](https://doi.org/10.1016/0011-7471(66)91102-8)

- MacIntyre, H. L., T. M. Kana, and R. J. Geider. 2000. The effect of water motion on short-term rates of photosynthesis by marine phytoplankton. *Trends Plant Sci.* **5**: 12–17. doi:[10.1016/S1360-1385\(99\)01504-6](https://doi.org/10.1016/S1360-1385(99)01504-6)
- Milligan, A. J., U. A. Aparicio, and M. J. Behrenfeld. 2012. Fluorescence and nonphotochemical quenching responses to simulated vertical mixing in the marine diatom *Thalassiosira weissflogii*. *Mar. Ecol. Prog. Ser.* **448**: 67–78. doi:[10.3354/meps09544](https://doi.org/10.3354/meps09544)
- Mitchell, B. G., and O. Holm-Hansen. 1991. Observations of modeling of the Antarctic phytoplankton crop in relation to mixing depth. *Deep-Sea Res. I Oceanogr. Res. Pap.* **38**: 981–1007. doi:[10.1016/0198-0149\(91\)90093-U](https://doi.org/10.1016/0198-0149(91)90093-U)
- Muller, P., X. P. Li, and K. K. Niyogi. 2001. Non-photochemical quenching. A response to excess light energy. *Plant Physiol.* **125**: 1558–1566. doi:[10.1104/pp.125.4.1558](https://doi.org/10.1104/pp.125.4.1558)
- Neale, P. J., E. W. Helbling, and H. E. Zagarese. 2003. Modulation of UVR exposure and effects by vertical mixing and advection, p. 107–134. *In* E. W. Helbling and H. E. Zagarese [eds.], *UV effects in aquatic organisms and ecosystems*. Comprehensive Series in Photochemical & Photobiological Sciences. Cambridge: The Royal Society of Chemistry. doi:[10.1039/9781847552266-00107](https://doi.org/10.1039/9781847552266-00107)
- Rudnick, D. L. 2016. Ocean research enabled by underwater gliders. *Ann. Rev. Mar. Sci.* **8**: 519–541. doi:[10.1146/annurev-marine-122414-033913](https://doi.org/10.1146/annurev-marine-122414-033913)
- Schofield, O., H. W. Ducklow, D. G. Martinson, M. P. Meredith, M. A. Moline, and W. R. Fraser. 2010. How do polar marine ecosystems respond to rapid climate change? *Science* **328**: 1520–1523. doi:[10.1126/science.1185779](https://doi.org/10.1126/science.1185779)
- Schofield, O., C. Jones, J. Kohut, U. Kremer, T. Miles, G. Saba, D. Webb, and S. Glenn. 2015. Developing coordinated communities of autonomous gliders for sampling coastal ecosystems. *Mar. Technol. Soc. J.* **49**: 9–16. doi:[10.4031/MTSJ.49.3.16](https://doi.org/10.4031/MTSJ.49.3.16)
- Schofield, O., and others. 2007. Slocum gliders: Robust and ready. *J. Field Robot.* **24**: 473–485. doi:[10.1002/rob.20200](https://doi.org/10.1002/rob.20200)
- Schofield, O., M. A. Moline, and B. B. Prezelin. 1995. Palmer LTER: Photoacclimation in a coastal phytoplankton bloom. *Antarctic Journal of the United States*. **30**(5): 260–262.
- Silsbe, G. M., and others. 2015. Toward autonomous measurements of photosynthetic electron transport rates: An evaluation of active fluorescence-based measurements of photochemistry. *Limnol. Oceanogr.: Methods* **13**: e10014. doi:[10.1002/lom3.10014](https://doi.org/10.1002/lom3.10014)
- Suggett, D. J., C. M. Moore, and R. J. Geider. 2010. Estimating aquatic productivity from active fluorescence measurements, p. 103–127. *In* *Chlorophyll a fluorescence in aquatic sciences: Methods and applications*. Springer.
- Suggett, D. J., C. M. Moore, A. E. Hickman, and R. J. Geider. 2009. Interpretation of fast repetition rate (FRR) fluorescence: Signatures of phytoplankton community structure versus physiological state. *Mar. Ecol. Prog. Ser.* **376**: 1–19. doi:[10.3354/meps07830](https://doi.org/10.3354/meps07830)
- Webb, W. L., M. Newton, and D. Starr. 1974. Carbon dioxide exchange of *Alnus rubra*. *Oecologia* **17**: 281–291. doi:[10.1007/BF00345747](https://doi.org/10.1007/BF00345747)
- Yentsch, C. S., and D. W. Menzel. 1963. A method for the determination of phytoplankton chlorophyll and phaeophytin by fluorescence. *Deep Sea Res. Oceanogr. Abstr.* **10**(3): 221–231. doi:[10.1016/0011-7471\(63\)90358-9](https://doi.org/10.1016/0011-7471(63)90358-9)

#### Acknowledgments

The authors would like to thank Rutgers field team (in particular to Nicole Couto, Nicole Waite, Mike Brown, and Chip Haldeman), Palmer Station personnel and ARSV Laurence M. Gould crew for support during deployments and recoveries. We would like to thank Kevin Wyman for his comments on the manuscript, Nathan Briggs for helpful discussions over data analyses and several anonymous reviewers for constructive comments. This work was supported by National Science Foundation (NSF Palmer LTER program, grant 0823101), National Oceanographic Partnership Program (NOPP, grant NA05OAR4601089), and NASA Ocean Biology and Biogeochemistry Program (grants NNX16AT54G and 80NSSC18K1416). Filipa Carvalho was funded by a Portuguese doctoral fellowship from Fundação para a Ciência e Tecnologia (FCT, grant DFRH - SFRH/BD/72705/2010), a Teledyne Marine Graduate Fellowship and a European Research Council Consolidator grant (GOCART, agreement number 724416).

#### Conflict of Interest

None declared.

Submitted 10 January 2020

Revised 21 June 2020

Accepted 24 June 2020

Associate editor: David Suggett